Larger earthquakes recur more periodically: new insights in the megathrust earthquake cycle from lacustrine turbidite records in south-central Chile

Moernaut, J.[a,d], Van Daele, M.[b], Fontijn, K.[c], Heirman, K.[b], Kempf, P.[b], Pino, M.[d], Valdebenito, G.[e], Urrutia, R.[f], Strasser, M.[a], De Batist, M.[b]

[a] Institute of Geology, University of Innsbruck, Innrain 52, Innsbruck, Austria

[b] Renard Centre of Marine Geology, Ghent University, Krijgslaan 281(S8), Gent, Belgium

[c] Department of Earth Sciences, University of Oxford, South Parks Road, Oxford, UK

[d] Instituto de Ciencias de la Tierra, Universidad Austral de Chile, Campus Isla Teja, Valdivia, Chile

[e] Instituto de Obras Civiles, Universidad Austral de Chile, Valdivia, Chile

[f] Centro EULA-Chile & Centro CRHIAM, Universidad de Concepción, Casilla 160-C, Concepción, Chile

Corresponding autor: Jasper.Moernaut@uibk.ac.at

Abstract

Historical and paleoseismic records in south-central Chile indicate that giant earthquakes on the subduction megathrust −such as in AD1960 (M_w9.5)− reoccur on average every ~300 years. Based on geodetic calculations of the interseismic moment accumulation since AD1960, it was postulated that the area already has the potential for a M_w8 earthquake. However, to estimate the probability of such a great earthquake to take place in the short term, one needs to frame this hypothesis within the long-term recurrence pattern of megathrust earthquakes in south-central Chile. Here we present two long lacustrine records, comprising up to 35 earthquake-triggered turbidites over the last 4800 years. Calibration of turbidite extent with historical earthquake intensity reveals a different macroseismic intensity threshold (≥VII½ vs. ≥VI½) for the generation of turbidites at the coring sites. The strongest

earthquakes (≥VII½) have longer recurrence intervals (292 ±93 yrs) than earthquakes with intensity of ≥VI½ (139 ±69 yrs). Moreover, distribution fitting and the coefficient of variation (CoV) of inter-event times indicate that the stronger earthquakes recur in a more periodic way (CoV: 0.32 *vs.* 0.5). Regional correlation of our multi-threshold shaking records with coastal paleoseismic data of complementary nature (tsunami, coseismic subsidence) suggests that the intensity ≥VII½ events repeatedly ruptured the same part of the megathrust over a distance of at least ~300 km and can be assigned to $M_w \geq 8.6$. We hypothesize that a zone of high plate locking –identified by geodetic studies and large slip in AD 1960– acts as a dominant regional asperity, on which elastic strain builds up over several centuries and mostly gets released in quasi-periodic great and giant earthquakes. Our paleo-records indicate that Poissonian recurrence models are inadequate to describe large megathrust earthquake recurrence in south-central Chile. Moreover, they show an enhanced probability for a M_w 7.7-8.5 earthquake during the next 110 years whereas the probability for a $M_w \geq 8.6$ (AD1960-like) earthquake remains low in this period.

Highlights

- Multi-threshold turbidite paleoseismic records in south-central Chilean lakes
- Probability estimates for $M_w \geq 7.7$ and $M_w \geq 8.6$ megathrust earthquakes
- Quasi-periodicity suggests a dominant role for a large megathrust asperity

Keywords

turbidite paleoseismology, south-central Chile, megathrust earthquake, seismic cycle, limnogeology

1. Introduction

Understanding the spatial and temporal recurrence pattern of large earthquakes is a crucial requisite for reliable seismic hazard assessments (Satake and Atwater, 2007). In addition to constraining the average recurrence rates for different magnitude classes, one needs to determine the best model for describing

53 the temporal aspect of the seismic cycle. Earthquake probabilities for a certain time window can be
54 calculated by fitting past recurrence times with a probabilistic density function. Due to the short
55 temporal span of seismological and historical data, and the typical uncertainties and assumptions
56 related to paleoseismic research, many challenges exist for integrating earthquake time series into
57 recurrence models (Wu et al., 1995). Quasi-periodic recurrence has been revealed for some fault-
58 specific cases, e.g. for the largest earthquakes on some isolated segments of major transform faults
59 (Scharer et al., 2010; Berryman et al., 2012). More complex transform fault systems may exhibit a
60 clustered recurrence, in which several short intervals alternate with much longer ones (Kenner and
61 Simons, 2005 and references therein). For some subduction megathrusts, analogue models and
62 paleoseismic studies suggest quasi-periodicity (Sykes and Menke, 2006; Corbi et al., 2013), which can be
63 modulated into “supercycles” in which a complete segment rupture ends a series of earthquakes of
64 varying magnitude (Goldfinger et al., 2013; Herrendörfer et al., 2015). Alternatively, time-independent
65 (Poissonian) recurrence models are found adequate to describe the recurrence of small earthquakes or
66 for analysis of regional seismic hazards (Wu et al., 1995; Gomez et al., 2015). Poissonian recurrence
67 models are commonly adopted for fault-specific cases where paleoseismic data is lacking.
68
69 Determination of the best recurrence model strongly depends on the “quality” of paleoseismic records:
70 i.e. the amount of recorded events, the dating accuracy, and information on paleo-earthquake size. In
71 lacustrine paleoseismology, several attempts have been made to constrain the local seismic intensity or
72 peak ground acceleration of paleo-earthquakes that are recorded in sedimentary sequences as soft-
73 sediment deformations, landslides, turbidites and post-seismic catchment responses (Strasser et al.,
74 2011; Howarth et al., 2014; Avsar et al., 2016; Wilhelm et al., 2016). In south-central Chile, previous
75 studies revealed strong relationships between seismic intensity during historical earthquakes, and type,
76 presence, thickness and extent of earthquake-triggered lacustrine turbidites (Moernaut et al., 2014; Van
77 Daele et al., 2015). This calibration of the sedimentary archive to historical events allowed defining a
78 site-specific earthquake recording threshold (EQRT), i.e. the minimal seismic intensity required to

produce a macroscopically visible turbidite at a given coring site. The studied sediment cores however only covered about 500-900 years and 5-7 events, and are thus not suited for deducing the temporal recurrence patterns of strong megathrust earthquakes.

Here, we present two long lacustrine turbidite records obtained in locations with different EQRTs and which contain up to 35 earthquake-triggered turbidites over the last 4800 years. This allows us –for the first time– to determine and compare the recurrence patterns of earthquake shaking of different intensity. Correlation with other records allows complementing the regional paleoseismic catalogue and putting forward possible seismo-tectonic mechanisms that explain the obtained recurrence patterns.

2. Setting and field data acquisition

Our study area is the Valdivia Segment of the subduction zone in south-central Chile (Fig. 1). Historical documents attest that this segment has been struck by four significant megathrust earthquakes (in AD1575, AD1737, AD1837 and AD1960) during the last ~500 years (Lomnitz, 1970; Cisternas et al., 2005). Combined with lacustrine (Moernaut et al., 2014) and coastal paleoseismic records (Cisternas et al., 2017), it was suggested that the megathrust earthquake cycle is characterized by a variable rupture mode in terms of rupture location, rupture extent and coseismic slip. Long coastal records revealed that the largest "1960-like" megathrust earthquakes and tsunamis occur on average every ~300 years, albeit with considerable temporal variability (Cisternas et al., 2005; Kempf et al., 2017). The AD1960 earthquake (M_w9.5) is notorious for having the highest instrumentally-recorded magnitude worldwide. It ruptured the subduction megathrust over about ~1000 km with an average slip of ~17 m, which peaked to ~44 m in an asperity at 40-41°S (Fig. 1; Moreno et al., 2009). Modeling of geodetic (GPS) data revealed a heterogeneous pattern of plate interface locking during the current interseismic period and it was postulated that several highly-locked patches may already be capable of producing a M_w8 earthquake (Moreno et al., 2011). However, to estimate the probability of such a great earthquake in

105 the near future, this hypothesis needs to be framed within the long-term recurrence pattern of
106 megathrust earthquakes in south-central Chile.
107
108 We studied the sedimentary infill of Lake Calafquén and Lake Riñihue, two large and deep glacigenic
109 lakes at the western foot of the volcanically active Andean Cordillera at 39.5-40°S latitude (Fig. 1; Fig. 2;
110 SI-Fig. 1). Previous studies on short sediment cores (0.5-1.5 m long) showed that the sedimentary infill
111 consists of annually-laminated hemipelagic sediments, interrupted by tephra layers, lahar deposits,
112 mass-transport deposits (MTD) and turbidites (Moernaut et al., 2014; Van Daele et al., 2014). Turbidites
113 in isolated sub-basins were accurately dated and analysis of their composition revealed that most of
114 these were produced by surficial remobilization of hemipelagic slope sediments during strong historical
115 earthquakes (Moernaut et al., 2017). The EQRT in these sub-basins was determined to range between
116 VI½ and VII½, with the lowest threshold values at the immediate foot of sedimentary slopes (Fig. 2;
117 Moernaut et al., 2014). For the present study, we obtained long sediment cores CAL1 (8.60 m) and RIN2
118 (7.25 m) with a hammer-driven piston coring system at short coring sites with an EQRT of VII½ and VI½,
119 respectively. This difference in EQRT is expressed by the absence of the AD1837, AD1737 and AD~1466
120 earthquakes in the short core of CAL1 (CASC01), whereas both sites contain turbidites related to the
121 AD1960, AD1575 and AD~1319 earthquakes (Fig. 3; Moernaut et al, 2014). The seismic-stratigraphic
122 characteristics at the coring sites were analyzed on high-resolution (3.5 kHz pinger) subbottom profiles,
123 making sure we selected the best coring location in terms of record continuity, i.e. avoiding -if possible-
124 any mass-transport deposits and hiatuses at the core site (SI-Fig.2).
125
126 **3. Data analysis**
127
128 Sedimentological analysis consisted of a detailed macro- and microscopic description, high-resolution
129 magnetic susceptibility and γ-density measurements using a GEOTEK core logger (details in Moernaut et
130 al., 2014). Turbidites were identified based on their homogeneous or fining-upwards characteristics,

131 which clearly contrast to the millimeter-scale laminations of the hemipelagic "background" sediments.
132 Smear slide analysis and magnetic susceptibility confirmed that the identified turbidites are composed
133 of diatomaceous mud produced by remobilization of hemipelagic slope sediments, and can be classified
134 as LT1s ("lacustrine turbidites type 1") after Van Daele et al. (2015). The sediments were dated using a
135 combined approach of i) varve counting (on the short cores) and identification of historical events (see
136 Moernaut et al., 2014), ii) AMS ^{14}C dating (SI-Table 1) and iii) geochemical identification of well-studied
137 regional tephra marker beds (SI-Table 1, Fontijn et al., 2016). The ^{14}C dating was performed on bulk
138 sediments and −where available− on macro-remains of terrestrial material. ^{14}C ages were calibrated
139 using the SHCal13 calibration curve (Hogg et al., 2013). The ^{14}C ages of the bulk sediment samples were
140 corrected for a soil-related "old-carbon" effect by subtracting the offset between the AD1575 historic
141 event and the weighted average of the calibrated ^{14}C age for bulk sediment at the corresponding depth
142 (SI-Table 1; see Moernaut et al., 2017). Regional marker tephras were identified in the studied cores and
143 on terrestrial outcrop samples by Fontijn et al. (2016), who used terrestrial samples for additional ^{14}C
144 dating and combined these to model the ages of tephras (mean age ±2σ) in a regional stratigraphic
145 framework.
146
147 All dates were used to produce a continuous age-depth model for each core using the Bayesian software
148 BACON (Fig. 4; Blaauw and Christen, 2011). All event layers (turbidites, tephras, lahars) were excluded
149 from the stratigraphic records. Turbidite ages were extracted from these models (SI-Table 2 and SI-Table
150 3) and inter-event times between (weighted mean) ages were analyzed by descriptive statistics. The
151 coefficient of variation "CoV" (i.e. the standard deviation divided by the mean) was used as a
152 straightforward characterization of the turbidite recurrence model: i.e. a CoV ~ 1 is associated to a
153 Poissonian distribution, CoV < 1 tends to quasi-periodicity, and CoV > 1 to clustered recurrence (as used
154 in Berryman et al., 2012). We further explored the goodness-of-fit (Kolmogorov-Smirnov test) of these
155 inter-event times to several types of probabilistic density functions commonly used in paleoseismic
156 research (Abaimov et al., 2008). The exponential distribution is characteristic for a Poissonian process,

157 which indicates that earthquakes occur randomly in time and the hazard rate remains constant.
158 Alternatively, quasi-periodicity may produce Normal, Log-normal or Weibull distributions for which the
159 hazard rate immediately after a large event is near zero and increases with time. Once the mean
160 recurrence time is exceeded, the shape of the hazard rate curve diverges between a continuous increase
161 (Weibull, Normal), or a tendency towards decreasing values (Log-normal). Log-logistic distributions can
162 point towards a clustered recurrence (Van Daele et al., 2014). It should be noted that the sample size
163 (34 and 12 recurrence times) is less than optimal for robust statistical analysis. However, given our well-
164 established age framework, we consider it reasonable to make a first-order descriptive characterization
165 and explore the goodness-of-fit for the mostly used distribution types.
166
167 This statistical analysis was also applied to a compiled catalogue of regional instrumental seismicity in
168 south-central Chile (SI-Table 4). We selected the timeframe 08/1999 to 02/2010, the latter date to avoid
169 the aftershock sequence of the AD2010 (M_w8.8) Maule earthquake. This catalogue includes interplate
170 and intraplate (oceanic plate or continental plate) earthquakes and contains M_w between 4.6 to 6.7
171 events. Due to the rather low seismicity registered in this region, we considered a rather large area (750
172 x 500 km; 36.5-43°S, 70.5-76°W).
173
174 **4. Turbidite records as paleoseismic proxy**
175
176 The long core in Lake Riñihue (RIN2) yields 7 regional tephra markers and 35 turbidites deposited during
177 the last 4700 years (Fig. 3; Fig. 4; SI-Fig. 3). One major volcanic deposit (~1 m thick) is associated to the
178 "Enco eruption" of the nearby Mocho-Choshuenco Volcano at 1587 ±58 cal yr BP ("V1" on Fig. 3; Fontijn
179 et al., 2016; Rawson et al., 2015). Turbidites ≤2 cm thick were considered "small" and relate to less
180 voluminous turbidity currents, as inferred by tracing the AD1837 and AD~1466 events on short core
181 transects (Moernaut et al., 2014). The long core in Lake Calafquén (CAL1) presents 2 regional tephra
182 markers and 13 turbidites deposited during the last 3500 years (Fig. 3; Fig. 4; SI-Fig. 4). Many thick lahar

deposits are present due to the vicinity of the highly-active snowcapped Villarrica Volcano (Fig. 2, Van Daele et al., 2014). The lowermost turbidite directly overlies a large mass-transport deposit (MTD), with a total thickness of about 4.5 m as determined on subbottom profiles. Seismic-stratigraphic analysis shows that this MTD was formed by coeval failure of at least four sedimentary slope segments surrounding the studied basin (SI-Fig. 2). Such a synchronous failure of subaquatic slopes is a typical fingerprint of strong earthquake shaking (e.g. Kremer et al., 2017).

We interpret an earthquake trigger for those lacustrine turbidites in CAL1 and RIN2 that are composed of remobilized hemipelagic sediments ("LT1s" of Van Daele et al., 2015). This inference is primarily based on the one-to-one correlation of LT1s with the strongest historical earthquakes, and the specific isolated setting of the studied subbasins. These basins lack significant river inflows and are morphologically protected from hyperpycnal flows originating from the main rivers bordering the deeper basins (Fig. 2). Moreover, many other trigger mechanisms for turbidity currents (i.e. alluvial fan collapses, lahars, propagation of onshore landslides, etc.) would result in a clearly more terrestrial composition of the turbidites and high magnetic susceptibility values ("LT2s" of Van Daele et al., 2015). We argue that the LT1 turbidites were exclusively produced by earthquakes within the Valdivia segment as the largest historical earthquakes on the adjacent Concepción Segment –such as the M_w8.8 earthquake in AD2010– failed to generate LT1 turbidites in either of the studied basins (Moernaut et al., 2014). The historical turbidites were all associated with megathrust earthquakes; however, it may be possible that local, intraplate earthquakes in prehistorical times have induced seismic intensities above VI½ and triggered turbidity currents at the studied basins.

It is generally assumed that subaquatic slope stability is governed by the rate at which sedimentary slopes are recharged with sediment between successive slope failure events (e.g. Strasser et al., 2011; Wilhelm et al., 2016). However, for the Chilean lakes, Moernaut et al. (2017) found that the turbidity currents associated to the AD1960 earthquake were produced by the remobilization of only a thin

209 veneer (few cm) of surficial slope sediments over large areas, and concluded that slope recharging after
210 a remobilization event plays only a minor role. They suggested that, as long as sedimentation rate and
211 sediment type remains relatively constant, the lacustrine turbidites have the potential to be sensitive
212 and continuous recorders of strong seismic shaking. As the Mid- to Late-Holocene records of RIN2 and
213 CAL1 present relatively stable sedimentation rates (Fig. 4) and constant sediment type (diatomaceous
214 mud), we further assume that the EQRTs as determined on short cores remained stable throughout the
215 entire time period here.
216
217 **5. Earthquake recurrence statistics**
218
219 The instrumental seismicity record is in accordance with a time-independent (Poissonian) process (Fig.
220 5A; Table 1), as expected for a regional record of small earthquakes. Poissonian recurrence is indicated
221 by a very good fit to an exponential distribution and a CoV of 1.1. In contrast, the turbidite inter-event
222 times of CAL1 and RIN2 have CoV values much lower than 1 (0.32 and 0.50, respectively) and the
223 goodness-of-fit test shows that the exponential distribution can be rejected at the 95% confidence level
224 (Table 1). Recurrence at the less sensitive site CAL1 averaged 292 (±93: standard deviation) years,
225 whereas RIN2 presents an average of 138 (±69) years. The normal distribution forms the best fit for
226 CAL1, which –together with the low CoV– points towards a quasi-periodic recurrence for earthquakes
227 that generated an intensity ≥VII½ at Lake Calafquén. For RIN2, the CoV value and the best fit to a
228 Weibull distribution also indicate a time-dependent recurrence behavior, albeit with a somewhat
229 weaker periodicity than for CAL1. The three datasets are compared on Fig. 5D by normalizing the
230 recurrence times over their mean value, and the cumulative number of observations. Visual comparison
231 confirms the exponential fit for the instrumental data, and the quasi-periodic character of the turbidite
232 records. The RIN2 distribution exhibits large tails at the shortest and longest recurrence times (red
233 arrows on Fig. 5D), whereas most of the data plots as close to its mean value as is the case for the CAL1
234 record.

It is generally assumed that large earthquakes occur at more regular time intervals when the causative fault is isolated from perturbing influences (Berryman et al., 2012). We suggest that the low CoV of 0.32 in the CAL1 record may result from repeated earthquakes on a single seismic source, on which rupture initiation takes place in a relatively isolated manner from other seismic sources in the region. Such a low CoV is remarkable when comparing turbidite paleoseismic records at different subduction zones. For example, marine turbidite records in Cascadia (Kulkarni et al., 2013), Sumatra (Patton et al. 2015) and Hikurangi (Pouderoux et al., 2014) show higher CoVs of about 0.5, 0.68 and 0.76, respectively. The lacustrine turbidite record in Lake Tutira (onshore Hikurangi) follows a Poissonian process characterized by an exponential distribution and a CoV of 1.05. This may result from a large number of potential subduction zone and crustal sources in the region that can generate strong shaking at the lake site (Gomez et al., 2014).

The choice of recurrence model can have significant implications for seismic hazard assessment. We explore this by calculating the earthquake probability since AD1960. Since then, no turbidites were recorded at the core sites of RIN2 and CAL1, due to an absence of significant earthquakes that generated an intensity ≥VI½ at the study sites (Moernaut et al., 2014). We used the turbidite records as input data and compared the commonly-used exponential distribution with the best fitting distribution (Weibull for RIN2; Normal for CAL1). The exponential model gives a probability of 33.7% and 17.7% for an event of ≥VI½ and ≥VII½, respectively, to have affected the area of the studied lakes between AD1960 and AD2017 (57 years). Best fitting distributions significantly lower this probability to 9.5% and 0.6%. Taking into account that no events with intensity ≥VI½ occurred in this period, the projections based on best fits show a much larger probability for an event of ≥VI½ (34.6%) within the next 57 years, whereas the probability for an event ≥VII½ remains rather low (2.2%).

6. Regional paleoseismic correlation

Correlation between our lacustrine paleoseismic records was performed by comparing the possible overlap of the age probability distributions of the events (Fig. 6). This reveals that the paleoseismic events in CAL1 (highest EQRT) have a high-probability counterpart in RIN2 (lower EQRT), as is expected due to the short distance between the lakes (~30 km) compared to the rupture length and location of great megathrust earthquakes (Fig. 1). The sole exception around ~1600 cal yr BP (Fig. 6) can be explained by the deposition of the thick volcanic layer "V1" at RIN2 (Fig. 3, 4; SI-Fig. 3), possibly obliterating any turbidite evidence. Alternatively, deformation the V1 deposit −as identified on the seismic profiles (SI-Fig. 2; SI-Fig. 3)− may be caused by the strong shaking recorded in CAL1. The small turbidites in RIN2 (<2cm thick, "S" on Fig. 6) were interpreted as the result of relatively weak seismic shaking near the EQRT of VI½ (Moernaut et al., 2014; 2017). This is well below the EQRT at CAL1 (VII½) and thus we do not expect these earthquakes to produce a turbidite there. This reasoning forms a useful correlation tool for the period before 2200 cal yr BP (Fig. 6B), where the short recurrence times in RIN2 and the broad age distributions in CAL1 complicate inter-lake correlations.

Several paleoseismic studies have been undertaken at the south-central Chilean coast. These consist of stratigraphic records of turbidites, tsunami deposits and/or evidence of coseismic elevation changes in coastal marshes and coastal lakes (summarized in Kempf et al., 2017 and Cisternas et al., 2017). Good agreements between records revealed four major earthquake ruptures in the last millennium, alternated by several smaller, more local earthquakes (Cisternas et al., 2017). Here, we extend the temporal span of regional correlation (Fig. 6) by comparing the new inland turbidite records and those coastal paleoseismic records that cover more than 1000 years, i.e. the Maullín site at 41.5°S (~2000 yrs; Cisternas et al., 2005) and the coastal Lake Huelde at 42.5°S (~5500 yrs; Kempf et al., 2017). We focus on the CAL1 site, as this relates to the strongest recorded intensities (AD1960-like; ≥VII½).

Comparison with the tsunami record in Lake Huelde for the last 2200 years (Fig. 6A) suggests an overall good correlation, with exception for one turbidite event (around 1400 cal yr BP) that lacks a tsunami, and one tsunami event (hI) without a turbidite counterpart in CAL1 (Fig. 6). Possible correlations back to 3600 cal yrs BP are more speculative due to limited age control on the records (Fig. 6B). Comparing CAL1 to the Maullín record (Cisternas et al., 2005), we find a striking one-to-one event correlation. Some earthquake events recorded in CAL1 are represented by either a tsunami or subsidence, whereas others seem to have been associated with both. This coherence between different types of paleoseismic data during the last 2000 years suggests that strong shaking (≥VII½) at the inland lake site CAL1 was exclusively produced by megathrust ruptures that also produced large tsunamis and/or significant coastal coseismic subsidence (typically ~1 m: Garret et al., 2015).

7. The role of asperities

The key idea of the subduction zone asperity model is that the largest megathrust earthquakes occur when large, strong regions (asperities) fail (Ruff, 1992). Such asperities are characterized by the largest coseismic slip values and may thus have accumulated the largest amounts of elastic strain during interseismic times. We hypothesize that asperity A1 (Fig. 6) is a persistent feature of high plate locking (>75%), where elastic strain builds up over several centuries, and which mostly gets released in large-slip earthquakes that occur quasi-periodically. This hypothesis is based on the combination of following observations:

a) The evidence for strong shaking (≥VII½) at the inland lakes is strongly correlated to large tsunami and/or significant coseismic subsidence ~250 km more to the south (coast of Maullín). This correlation partially extends to evidence for tsunamis ~380 km southwards of the inland lakes (coastal Lake Huelde). This regional correlation suggests the occurrence of long (>250 km) ruptures of the megathrust, the location of which corresponds to the A1 area.

312

313 b) The A1 area was characterized by the highest amount of coseismic slip in AD1960 (up to ~44 m). In
314 the asperity model, this requires an extended, mechanically strong patch on the megathrust.

315

316 c) The A1 area is generally characterized by a high degree of locking (>75%) of the plate interface (Fig. 6;
317 Moreno et al., 2011). Such effective locking allows rapid accumulation of elastic strain and recharges the
318 asperity for rupture during future earthquakes. Lower locking degree would result in either postponed
319 and/or smaller megathrust earthquakes, which then would fail to explain the 300 year cycle of large-slip
320 AD1960-like megathrust earthquakes.

321

322 d) By comparing the hypothetically accumulated moment deficit for a 300-year seismic cycle and the
323 released coseismic moment in AD1960, Moreno et al. (2011) suggested that the locking distribution may
324 evolve through time or that some asperities are not persistent over multiple earthquake cycles.
325 However, from the elapsed time between AD1575 and AD1960, Moernaut et al. (2014) proposed that
326 the AD1837 earthquake may eliminate the discrepancies in the moment budget and, consequently, that
327 the locking distribution may have been rather stable since at least AD1575.

328

329 e) The low CoV of the CAL1 record (intensity ≥VII½) suggests that the earthquake source that generated
330 these turbidites is a simple, isolated structure for which the seismic cycle is little affected by other fault
331 activity in the region (see section 5). For a subduction zone with heterogeneous locking and variable
332 rupture mode, we postulate that this is only feasible when an extended strongly-coupled source area is
333 bordered by zones of significant weaker coupling, allowing a certain degree of independence of seismic
334 cycles on adjacent segments. Indeed, Moreno et al. (2011) model a locking ratio of only ~0.5-0.6 at the
335 northern and southern limits of the A1 area. However, we believe that the independency of the A1
336 seismic cycle is weakened by possible multi-segment ruptures initiating elsewhere on the megathrust
337 (e.g. in AD1960) and static stress changes imposed by adjacent segments. Such interferences may have

338 increased the CoV to 0.32 compared to what is expected for a truly isolated fault segment (CoV: 0.1-0.3;
339 see Sykes and Menke, 2006).
340
341 Rupturing a subduction megathrust with dimensions of the A1 patch and immediate surroundings (~370
342 x 160 km), such as the near-trench area, is estimated to result in a M_w~8.6 earthquake (Allen and Hyes,
343 2017). This estimate is justified by the intermediate dimensions of the A1 patch compared to well-
344 characterized larger and smaller Chilean megathrust ruptures during the last decade: i.e. the AD2010
345 Maule (M_w8.8, ~460 km long), AD2014 Iquique (M_w8.1; ~130 km long) and AD2015 Illapel (M_w8.4, ~130
346 km long) earthquakes. It is important to note that the magnitude value of M_w8.6 is a minimum estimate
347 because ruptures of past events may have propagated far beyond the extent of the A1 patch and
348 because very large coseismic slip (~44 m) is physically possible on A1, as illustrated by the AD1960
349 event.
350
351 For the turbidite record at the RIN2 site, we estimate a lower magnitude bound of M_w7.7 for causative
352 megathrust events, in accordance with the magnitude estimate of the historical AD1737 event (Lomnitz,
353 1970). This event produced rather restricted turbidites in Lake Riñihue, which just reached site RIN2 (see
354 short core "RI2" in Moernaut et al., 2014). Besides large-slip ruptures of the A1 patch, as recorded in
355 CAL1, the RIN2 site may also have registered smaller earthquakes at different sections of the megathrust
356 or –in minor amount− from other seismic sources, such as events in the downgoing plate or in the
357 continental crust (discussed in Moernaut et al., 2014). These largely independent processes may lead to
358 unexpected short recurrence times between turbidites, producing the lower tail in the distribution (Fig.
359 5D). The RIN2 distribution tail at large recurrence times is close to the mean recurrence of CAL1, which
360 suggests that several periods existed in which no M_w7.7-8.5 earthquakes took place between successive
361 $M_w \geq 8.6$ events.
362

363 Taking into account the abovementioned assumptions and simplifications, we state that our multi-site
364 approach provides information about the recurrence of earthquakes above different magnitude
365 thresholds. For $M_w \geq 8.6$ earthquakes, we confirm the average recurrence rate of 285 years for AD1960-
366 like earthquakes obtained by Cisternas et al. (2005) and refine it to 292 (±93) years. Such ruptures of the
367 largest/strongest asperities on the megathrust seem to happen in a quasi-periodical manner. A lower
368 magnitude threshold of $M_w \geq 7.7$ yields shorter recurrence times with more variability (138 ±69 yrs). Our
369 observation that periodicity increases with larger magnitudes is in accordance with simulated
370 earthquake catalogues for varying degrees of fault system complexity (Dieterich and Richards-Dinger,
371 2010), and thus we suggest that a quasi-periodic recurrence can be a typical feature for the largest
372 earthquakes on a given (isolated) fault segment or asperity.
373
374 Previous historical and paleoseismic studies inferred that the Valdivia segment is characterized by a
375 variable rupture mode in terms of rupture extent, location and slip (Moernaut et al., 2014; Cisternas et
376 al., 2017). The inter-lake correlation (Fig.6) shows that 0 to 3 (average of 1.3) smaller events (M_w 7.7-8.5)
377 took place between the M_w>8.6 earthquakes. The megathrust thus exhibits a weak supercycle behavior
378 compared to e.g. the Tohoku area (NE Japan) where historical and paleotsunami records suggested
379 longer recurrence intervals (~600 years) for the largest events (M_w 8.5-9) and much shorter recurrence
380 intervals (~37 years) for the intermittent smaller earthquakes (Satake, 2015). Compared to the Cascadia
381 margin (Goldfinger et al., 2013) or Sunda megathrust (Philibosian et al., 2017), our records seem to lack
382 the long quiescence periods (relative to the average interval) that mark the start of a supercycle. A
383 possible exception may be the ~330-year long interval from 1180-850 cal yr BP when no earthquakes
384 larger than M_w7.6 were recorded in our study area (Fig. 6). It is important to note that paleoseismic
385 records at the northern limit of the Valdivia Segment are limited to only ~500 years (Ely et al., 2014) and
386 no records exist for the southern third of the Valdivia Segment. Consequently, we cannot constrain the
387 rupture extents of the inferred paleo-earthquakes and inferences about super-events (i.e. full segment
388 ruptures) remain speculative.

389

390 Our paleoseismic records allow us to re-evaluate the hypothesis of Moreno et al. (2011); i.e. whether
391 the Valdivia Segment is already prone to a new M_w8 earthquake. Considering the M_w7.7 threshold
392 (RIN2), we find that the shape of the best fitting distribution (Weibull; Fig.5) illustrates an enhanced
393 probability (probability density > 0.25) for such events to occur when ~65-175 years passed since the
394 latest event. To date, 57 years have elapsed since AD1960 and thus a M_w8 event in the next ~110 years
395 is a likely scenario (70.0% probability). For the next 50 years –a time interval often used in seismic
396 hazard assessments– the probability is 29.5%. The three shortest inter-event times in RIN2 were ~34, 50
397 and 52 years, suggesting that a new $M_w \geq 7.7$ event in the short term is not impossible from a paleo-
398 perspective. In contrast, the probability for a new $M_w \geq 8.6$ earthquake to occur in the next 110 years
399 remains low (8.4%). It is important to note that these calculations are solely based on time series and do
400 not take into account the (M_w8.8) AD2010 rupture of the Concepción segment (Fig. 1), which may have
401 initiated a "super-interseismic phase" at the adjacent segments north and south of it (discussed in
402 Melnick et al., 2017). It is believed that such enhanced coupling provoked a reawakening of large
403 megathrust earthquakes in the Valdivia Segment (Ruiz et al., 2017), illustrated by the recent 25-12-2016
404 (M_w 7.6) Chiloé event, which terminated a period of only small- to moderate-magnitude seismicity since
405 the (M_w 9.5) AD1960 earthquake and its aftershocks.
406

407 **8. Conclusions**

408

409 • Multi-threshold shaking records can be obtained from lacustrine turbidite sequences by careful
410 core site selection and determination of intensity thresholds via historical calibration. Such
411 records allow comparing the recurrence patterns of great and giant earthquakes at subduction
412 zones. For south-central Chile, our records show an average recurrence rate of 292 ±93 years
413 and 139 ±69 years for $M_w \geq 8.6$ and $M_w \geq 7.7$ earthquakes, respectively. $M_w \geq 8.6$ earthquakes
414 reoccur in a more periodic manner than smaller ones.

- Poissonian recurrence models are not adequate to describe large megathrust earthquakes in south-central Chile, and probabilistic seismic hazard assessments should include a time-dependent approach. We infer that the $M_w \geq 8.6$ and $M_w \geq 7.7$ earthquake series best fit to a Normal and Weibull distribution, respectively, which means that the hazard rate rises with time.
- Our paleo-records allow us to confirm the statement of Moreno et al. (2011) that a M_w8 megathrust earthquake is already possible in the Valdivia segment, even though only 57 years have passed since the giant AD1960 earthquake. We find that there is an enhanced probability for such event during the next 110 years. The probability for a new $M_w \geq 8.6$ (1960-like) earthquake however remains low in this period.
- Temporal correlation of multiple types of paleoseismic evidence over more than 300 km let us suggest that a zone of high interseismic locking and large coseismic slip in AD1960 can be considered as a persistent asperity, which dominantly controls the quasi-periodic reoccurrence of the largest megathrust events ($M_w \geq 8.6$).
- Paleoseismic records allow evaluating the long-term role of asperities −identified by GPS surveys and punctual coseismic slip distributions− in shaping the seismic hazard of a region. A better spatial coverage of multi-threshold lacustrine paleoseismic records and integration with more (and longer) paleoseismic archives of different nature are needed to fully explore the spatial and temporal patterns of megathrust recurrence in south-central Chile.

Acknowledgements:

JM acknowledges financial support from a research grant from the University of Innsbruck (Nachwuchsförderung 2016), the Chilean Fondecyt projects no. 1150346 and 1150321, and the Swiss National Science Foundation (grant 133481); MVD and MDB from the Research Foundation – Flanders (FWO); MP and GV from the UACh excellence centres TAQUACH and RINA (Natural and Anthropogenic Risks Research Center Chile); RU from project CRHIAM /CONICYT/FONDAP/15130015; KF from the UK's

441 Natural Environment Research Council (grants NE/I013210/1 and NE/L013921/1). IHS Kingdom is
442 acknowledged for their educational grant program providing seismic interpretation software. We thank
443 Koen De Rycker, Alejandro Peña, Javiera Cardenas, Rolf Kilian and Marcelo Arévalo for technical and
444 logistical support. Dr. Mike Clare and Dr. Marco Cisternas are thanked for fruitful discussions about the
445 interpretation of the paleoseismic data. We gratefully thank Alina Polonia and an anonymous reviewer
446 for their constructive comments on an earlier version of this manuscript.
447

448 **Figure captions:**

449

450 Fig. 1: A) Rupture area and estimated coseismic slip of the largest megathrust earthquakes in the
451 Valdivia Segment in south central Chile, derived from a compilation of instrumental, historical and
452 paleoseismic data (Moernaut et al., 2014). The location of the AD2016 earthquake (M_w 7.6) is derived
453 from the aftershock distribution registered by the Centro Sismológico Nacional de Chile. B) Tectonic
454 setting of south-central Chile with indication of coseismic slip in AD1960 (red contour lines; Moreno et
455 al., 2009) and areas of high locking ratio (>75%, in grey) along the megathrust (Moreno et al., 2011).
456 Note that the largest slip in AD1960 (40-41°S) corresponds to a highly locked area. LOFZ: Liquiñe-Ofqui
457 Fault Zone. Triangles: Holcene and/or historically active volcanoes (Global Volcanism Program;
458 http://volcano.si.edu). Va: Valdivia, Co: Concepción.

459

460 Fig. 2: A) local setting of study lakes Riñihue and Calafquén with indication of active volcanoes and the
461 lakes´ sedimentary (white curve) and fluvial catchments (dashed white curve). We studied the
462 sedimentary infill of distal basins in the western parts of the lakes. Bathymetry of the lakes on SI-Fig.1. B
463 and C) Earthquake-recording threshold (EQRT) for lacustrine turbidites type 1 (LT1s: see Moernaut et al.,
464 2014) of several short coring sites (white dots) in the studied lakes. Note that the long core sites CAL1
465 and RIN2 (red dots) are characterized by a different EQRT. Bathymetric contours every 10m.

466

Fig. 3. Left) Short cores at long core site RIN2 (RINSC07) and CAL1 (CASC01) with indication of lacustrine turbidites (blue) triggered by major historical and prehistorical earthquakes (modified after Moernaut et al., 2014). Yellow curve depicts the magnetic susceptibility of the sediments. Color variability of the core pictures was enhanced using histogram equalization. Due to its lower EQRT, RINSC07 contains more turbidites during the last 700 years compared to CASC01. Right) Composite log of long cores RIN2 and CAL1 with indication of turbidites (blue, numbered) and volcanic deposits. Core-to-seismic correlation is presented on Si-Fig.2. Logs of individual core segments can be found on SI-Fig.3 and Si-Fig.4 and includes magnetic susceptibility, γ-density, regional marker tephras and ^{14}C dated levels.

Fig. 4: Age-depth models for RIN2 and CAL1 constructed with BACON software. Event deposits (turbidites, tephras, lahars) were excluded before modeling. Data for each input age can be found in SI-Table 1.

Fig. 5: A-C) Histograms for recurrence times in the instrumental record, RIN2 and CAL1, with indication of the present-day situation ("2017AD"). The three main distribution types in this study are plotted for each dataset. D) Normalized recurrence data for the three records for visual comparison between distribution shapes (see legend).

Fig. 6: Compilation of event timing for long (>1000 yrs) paleoseismic records in the Valdivia Segment (see also Kempf et al., 2017). Fig. 6A shows the last 2200 years whereas Fig. 6B covers the period 5400-2200 cal yr BP. Yellow areas on the map correspond to a locking ratio >75% as calculated by Moreno et al. (2001). We define asperity "A1" as the >75% locked zone between 39.5-42.5°S. V1 is a large volcanic deposit in RIN2 including some soft-sediment deformations (corresponding to the Enco eruption of Mocho-Choshuenco; Rawson et al. 2015; Fontijn et al. 2016; SI-Fig. 3). "S" in RIN2 corresponds to small turbidites with thickness less than 2 cm. Color coding illustrates the suggested correlations. Different types of paleoseismic evidence are given by symbols (see legend).

493

494 Table 1: Statistical analysis of recurrence times in the instrumental record, RIN2 and CAL1. This includes
495 descriptive statics and a goodness-of-fit test for different probability density distributions. The null
496 hypothesis is that the observed data follow the specified distribution. The null hypothesis can be
497 rejected when the test statistic is lower than a critical value. Distribution fits that can be rejected at the
498 95% confidence level are indicated by "(R)". Lower p-values indicate that a certain distribution can be
499 rejected at a higher confidence level. We select the most likely distribution (marked in bold) as the one
500 with lowest test statistic value and highest p-value.

501

References:

Abaimov, S.G., Turcotte, D.L., Shcherbakov, R., Rundle, J.B., Yakovlev, G., Goltz, C., Newman, W.I., 2008. Earthquakes: recurrence and interoccurrence times. Pure appl. Geophys. 165, 777-795. doi:10.1007/s00024-008-0331-y

Allen, T.I., Hayes, G.P., 2017. Alternative rupture-scaling relationships for subduction interface and other offshore environments. Bull. Geol. Soc. Am. 107(3), doi:10.1785/0120160255

Avsar, U., Jonsson, S., Avsar, Ö., Schmidt, S., 2016. Earthquake-induced soft-sediment deformations and seismically amplified erosion rates recorded in varved sediments of Köyceğiz Lake (SW Turkey). J. Geophys. Res.-Sol. Ea. 121(6), 4767-4779. doi:10.1002/2016JB012820.

Berryman, K.R., Cochran, U.A., Clark, K.J., Biasi, G.P., Langridge, R.M., Villamor, P., 2012. Major earthquakes occur regularly on an isolated plate boundary fault. Science 336, 1690-1693. doi:10.1126/science.1218959

Blaauw, M., Christen, J.A., 2011. Flexible paleoclimate age-depth models using an autoregressive gamma process. Bayesian Anal. 6, 457-474. doi:10.1214/11-BA618

Cisternas, M., Atwater, B.F., Torrejon, F., Sawai, Y., Machuca, G., Lagos, M., Eipert, A., Youlton, C., Salgado, I., Kamataki, T., Shishikura, M., Rajendran, C.P., Malik, J.K., Rizal, Y., and Husni, M., 2005. Predecessors of the giant 1960 Chile earthquake. Nature 437, 404-407. doi:10.1038/nature03943

526 Cisternas, M., Garrett, E., Wesson, R., Dura, T., Ely, L.L., 2017. Unusual geologic evidence of coeval
527 seismic shaking and tsunamis shows variability in earthquake size and recurrence in the area of the giant
528 1960 Chile earthquake. Mar. Geol. 385, 101-113. doi:10.1016/j.margeo.2016.12.007
529
530 Corbi, F., Funiciello, F., Moroni, M., van Dinther, Y., Mai, P.M., Dalguer, L.A., Faccenna, C., 2013. The
531 seismic cycle at subduction thrusts: 1. Insights from laboratory models. J. Geophys. Res.-Sol. Ea. 118(4),
532 1483-1501. doi:10.1029/2012JB009481
533
534 Dieterich, J.H., Richards-Dinger, K.B., 2010. Earthquake recurrence in simulated fault systems. Pure and
535 Appl. Geophys. 167, 1087-1104. doi: 10.1007/s00024-010-0094-0
536
537 Ely, L.L., Cisternas, M., Wesson, R.L., Dura, T., 2014. Five centuries of tsunamis and land-level changes in
538 the overlapping rupture area of the 1960 and 2010 Chilean earthquakes. Geology 42(11), 995-998.
539 doi: 10.1130/G35830.1
540
541 Fontijn, K., Rawson, H., Van Daele, M., Moernaut, J., Abarzúa, A.M., Heirman, K., Bertrand, S., Pyle, D.M.,
542 Mather, T.A., De Batist, M., Naranjo, J.-A., Moreno, H., 2016. Synchronisation of sedimentary records
543 using tephra: A postglacial tephrochronological model for the Chilean Lake District. Quaternary Sci. Rev.
544 137, 234-254. doi:10.1016/j.quascirev.2016.02.015
545
546 Garret, E., Schennan, I., Woodroffe, S.A., Cisternas, M., Hocking, E.P., Gulliver, P., 2015. Reconstructing
547 paleoseismic deformation, 2: 1000 years of great earthquakes at Chucalén, south central Chile.
548 Quaternary Sci. Rev. 113, 112-122. doi:10.1016/j.quascirev.2014.10.010
549
550 Goldfinger, C., Ikeda, Y., Yeats, R., Ren, J., 2013. Superquakes and supercycles. Seismol. Res. Lett. 84(1),
551 1-9. doi:10.1785/0220110135

552

553 Gomez, B., Corral, A., Orpin, A.R., Page, M.J., Pouderoux, H., Upton, P., 2015. Lake Tutira paleoseismic
554 record confirms random, moderate to major and/or great Hawke's Bay (New Zealand) earthquakes.
555 Geology 43(2), 103-106. doi:10.1130/G36006.1

556

557 Herrendörfer, R., van Dinther, Y., Gerya, T., Dalguer, L.A., 2015. Earthquake supercycle in subduction
558 zones controlled by the width of the seismogenic zone, Nat. Geosci. 8, 471-475. doi:10.1038/NGEO2427

559

560 Hogg, A.G., Hua, Q., Blackwell, P.G., Niu, M., Buck, C.E., Guilderson, T.P., Heaton, T.J., Palmer, J.G.,
561 Reimer, P.J., Reimer, R.W., Turney, C.S.M., Zimmerman, S.R.H., 2013. SHCal13 southern hemisphere
562 calibration, 0–50,000 years cal BP. Radiocarbon 55 (4), 1889-1903. doi:10.2458/azu_js_rc.55.16783.

563

564 Howarth, J., Fitzsimons, S.J., Norris, R.J., Jacobsen, G.E., 2014. Lake sediments record high intensity
565 shaking that provides insight into the location and rupture length of large earthquakes on the Alpine
566 Fault, New Zealand. Earth Planet. Sc. Lett. 402, 340-351. doi:10.1016/j.epsl.2014.07.008

567

568 Kempf, P., Moernaut, J., Van Daele, M., Vandoorne, W., Pino, M., Urrutia, R., De Batist, M., 2017. Coastal
569 lake sediments reveal 5500 years of tsunami history in south central Chile. Quaternary Sci. Rev. 161, 99-
570 116. doi: 10.1016/j.quascirev.2017.02.018

571

572 Kenner, S.J., Simons, M., 2005. Temporal clustering of major earthquakes along individual faults due
573 to post-seismic reloading. Geophys. J. Int. 160, 179-194. doi: 10.1111/j.1365-246X.2005.02460.x

574

575 Kremer, K., Wirth, S.B., Reusch, A., Fäh, A., Bellwald, B., Anselmetti, F.S., Girardclos, S., Strasser, M.,
576 2017. Quaternary Science Reviews 168, 1-18. doi: 10.1016/j.quascirev.2017.04.026

577

578 Kulkarni, R., Wong, I., Zachariasen, J., Goldfinger, C., Lawrence, M., 2013. Statistical analyses of great
579 earthquake recurrence along the Cascadia subduction zone. B. Seismol. Soc. Am. 103(6), 1-17.
580 doi:10.1785/0120120105
581
582 Lomnitz, C., 1970. Major earthquakes and tsunamis in Chile during the period 1535 to 1955. Geol.
583 Rundsch. 59, 938-960. doi:10.1007/BF02042278
584
585 Melnick, D., Moreno, M., Quinteros, J., Baez, J.C., Deng, Z., Li, S., Oncken, O., 2017. The super-
586 interseismic phase of the megathrust earthquake cycle in Chile. Geophys. Res. Lett. 44, 784-791.
587 doi:10.1002/2016GL071845
588
589 Moernaut, J., Van Daele, M., Heirman, K., Fontijn, K., Strasser, M., Pino, M., Urrutia, R., De Batist, M.,
590 2014. Lacustrine turbidites as a tool for quantitative earthquake reconstruction: New evidence for a
591 variable rupture mode in south central Chile, J. Geophys. Res.-Sol. Ea. 119, 1607-1633,
592 doi:10.1002/2013JB010738.
593
594 Moernaut, J., Van Daele, M., Strasser, M., Clare, M.A., Heirman, K., Viel, M., Cardenas, J., Kilian, R.,
595 Ladrón de Guevara, B., Pino, M., Urrutia, R., De Batist, M., 2017. Lacustrine turbidites produced by
596 surficial slope sediment remobilization: a mechanism for continuous and sensitive turbidite paleoseismic
597 records. Mar. Geol. 384, 159-176. doi:10.1016/j.margeo.2015.10.009
598
599 Moreno, M.S., Bolte, J., Klotz, J., Melnick, D., 2009. Impact of megathrust geometry on inversion of
600 coseismic slip from geodetic data: Application to the 1960 Chile earthquake. Geophys. Res. Lett. 36,
601 L16310. doi:10.1029/2009GL039276
602

603 Moreno, M., Melnick, D., Rosenau, M., Bolte, J., Klotz, J., Echtler, H., Baez, J., Bataille, K., Chen, J., Bevis,
604 M., Hase, H., Oncken, O., 2011. Heterogeneous plate locking in the South-Central Chile subduction zone:
605 Building up the next great earthquake. Earth Planet. Sc. Lett. 305(3-4), 413-424.
606 doi:10.1016/j.epsl.2011.03.025
607
608 Patton, J.R., Goldfinger, C., Morey, A.E., Ikehara, K., Romsos, C., Stoner, J., Djadjadihardja, Y., Udrekh,
609 Ardhyastuti, S., Gaffar, E.Z., Vizcaino, A., 2015. A 6600 year earthquake history in the region of the 2004
610 Sumatra-Andaman subduction zone earthquake: Geosphere 11 (6), 1-63. doi:10.1130/GES01066.1.
611
612 Philibosian, B., Sieh, K., Avouac, J.-P., Natawidjaja, D.H., Chiang, H.-W., Wu, C.-C., Shen, C.-C., Daryono,
613 M.R., Perfettini, H., Suwargadi, B.W., Lu, Y., Wang, X., 2017. Earthquake supercycles on the Mentawai
614 segment of the Sunda megathrust in the seventeenth century and earlier. J. Geophys. Res.-Sol. Ea. 122,
615 642-676, doi:10.1002/2016JB013560
616
617 Pouderoux, H., Proust, J.-N., Lamarche, G., 2014. Submarine paleoseismology of the northern Hikurangi
618 subduction margin of New Zealand as deduced from turbidite record since 16 ka. Quaternary Sci. Rev.
619 84, 116-131. doi:10.1016/j.quascirev.2013.11.015
620
621 Rawson, H., Naranjo, J.-A., Smith, V., Fontijn, K., Pyle, D.M., Mather, T.A., Moreno, H., 2015. The
622 frequency and magnitude of post-glacial explosive eruptions at Volcán Mocho-Choshuenco, southern
623 Chile. J. Volcanol. Geotherm. Res. 299, 103-129. doi:10.1016/j.jvolgeores.2015.04.003
624
625 Ruff, L.J., 1992. Asperity distributions and large earthquake occurrence in subduction zones.
626 Tectonophysics 211, 61-83. doi:10.1016/0040-1951(92)90051-7
627
628 Ruiz, S., Moreno, M., Melnick, D., del Campo, F., Poli, P., Baez, J.C., Leyton, F., Madariaga, R., 2017.

629 Reawakening of large earthquakes in south central Chile: The 2016 Mw 7.6 Chiloé event. Geophys.
630 Res. Lett. 44, doi:10.1002/2017GL074133
631
632 Satake, K., Atwater, B.F., 2007. Long-term perspectives on giant earthquakes and tsunamis at
633 subduction zones. Annu. Rev. Earth Pl. Sc. 35, 349-274. doi:10.1146/annurev.earth.35.031306.140302
634
635 Satake, K., 2015. Geological and historical evidence of irregular recurrent earthquakes in Japan. Phil.
636 Trans. R. Soc. A 373, 20140375. doi: 10.1098/rsta.2014.0375
637
638 Scharer, K.M., Biasi, G.P., Weldon, R.J., Fumal, T.E., 2010. Quasi-periodic recurrence of large earthquakes
639 on the southern San Andreas fault. Geology 38(6), 555-558. doi:doi.org/10.1130/G30746.1
640
641 Strasser, M., Hilbe, M., Anselmetti, F.S., 2011. Mapping basin-wide subaquatic slope failure susceptibility
642 as a tool to assess regional seismic and tsunami hazards. Mar. Geophys. Res. 32 (1-2), 331-347.
643 doi:10.1007/s11001-010-9100-2
644
645 Sykes, L.R., Menke, W., 2006. Repeat times of large earthquakes: implications for earthquake mechanics
646 and long-term prediction. B. Seismol. Soc. Am. 96(5), 1569-1596, doi: 10.1785/0120050083
647
648 Van Daele, M., Moernaut, J., Silversmit, G., Schmidt, S., Fontijn, K., Heirman, K., Vandoorne, W., De
649 Clercq, M., Van Acker, J., Wolff, C., Pino, M., Urrutia, R., Roberts, S.J., Vincze, L., De Batist, M., 2014. The
650 600 yr eruptive history of Villarrica Volcano (Chile) revealed by annually laminated lake sediments. Geol.
651 Soc. Am. Bull. 126(3-4), 481-498. doi: 10.1130/B30798.1
652
653 Van Daele, M., Moernaut, J., Doom, L., Boes, E., Fontijn, K., Heirman, K., Vandoorne, W., Hebbeln, D.,
654 Pino, M., Urrutia, R., Brümmer, R., De Batist, M., 2015. A comparison of the sedimentary records of the

1960 and 2010 great Chilean earthquakes in 17 lakes: implications for quantitative lacustrine paleoseismology. Sedimentology, 62(5), 1466-1496. doi:10.1111/sed.12193

Wilhelm, B., Nomade, J., Crouzet, C., Litty, C., Sabatier, P., Belle, S., Rolland, Y., Revel, M., Courboulex, F., Arnaud, F., Anselmetti, F.S., 2016. Quantified sensitivity of small lake sediments to record historic earthquakes: Implications for paleoseismology. J. Geophys. Res.-Earth 121(1), 2-16. doi:10.1002/2015JF003644

Wu, S.-C., Cornell, C.A., Winterstein, S.R., 1995. A hybrid recurrence model and its implication on seismic hazard results. B. Seismol. Soc. Am. 85(1), 1-16.

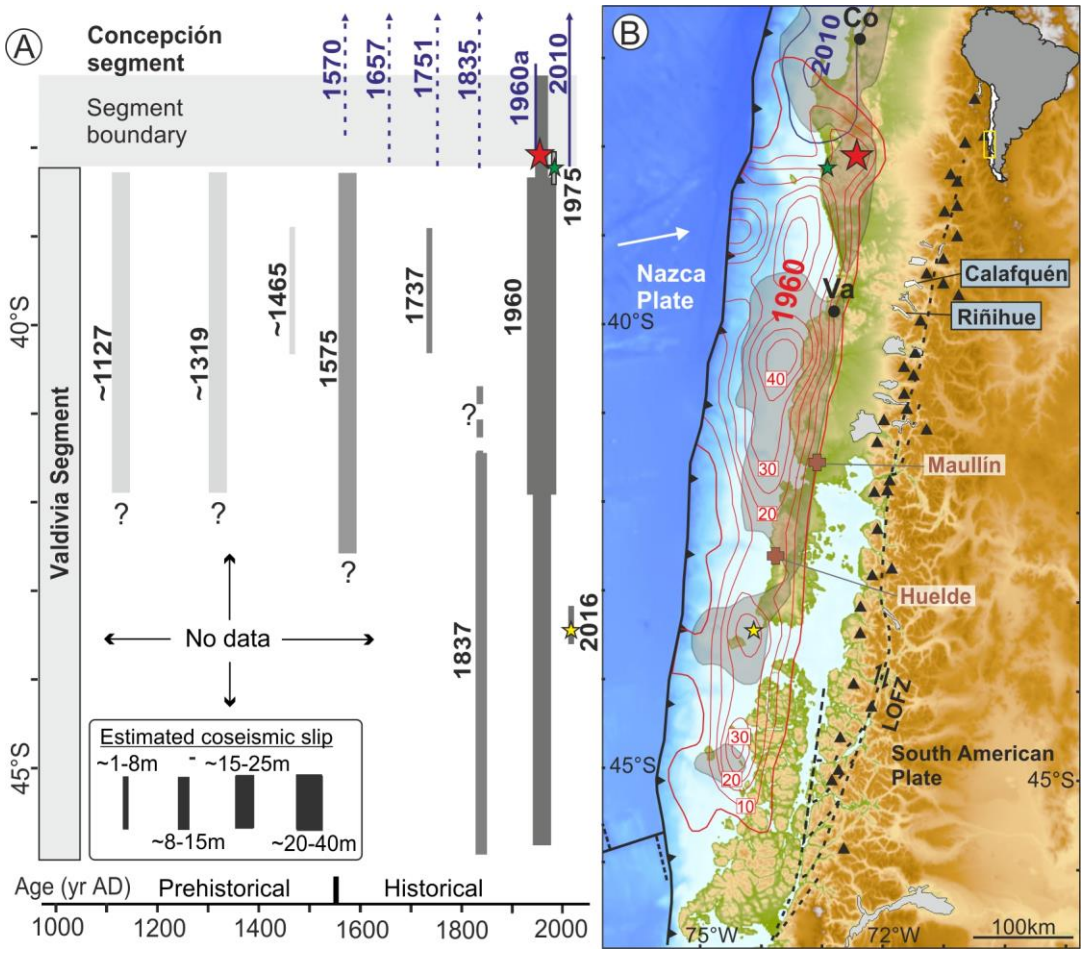

Figure 1

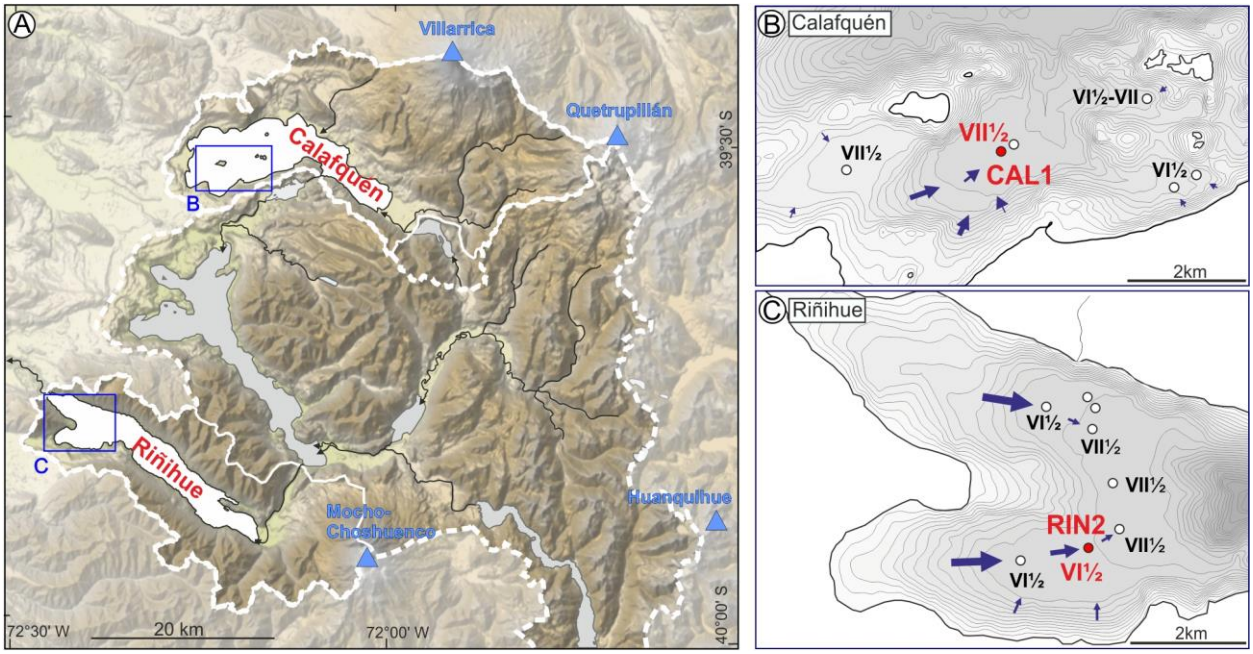

668

669 **Figure 2**

670

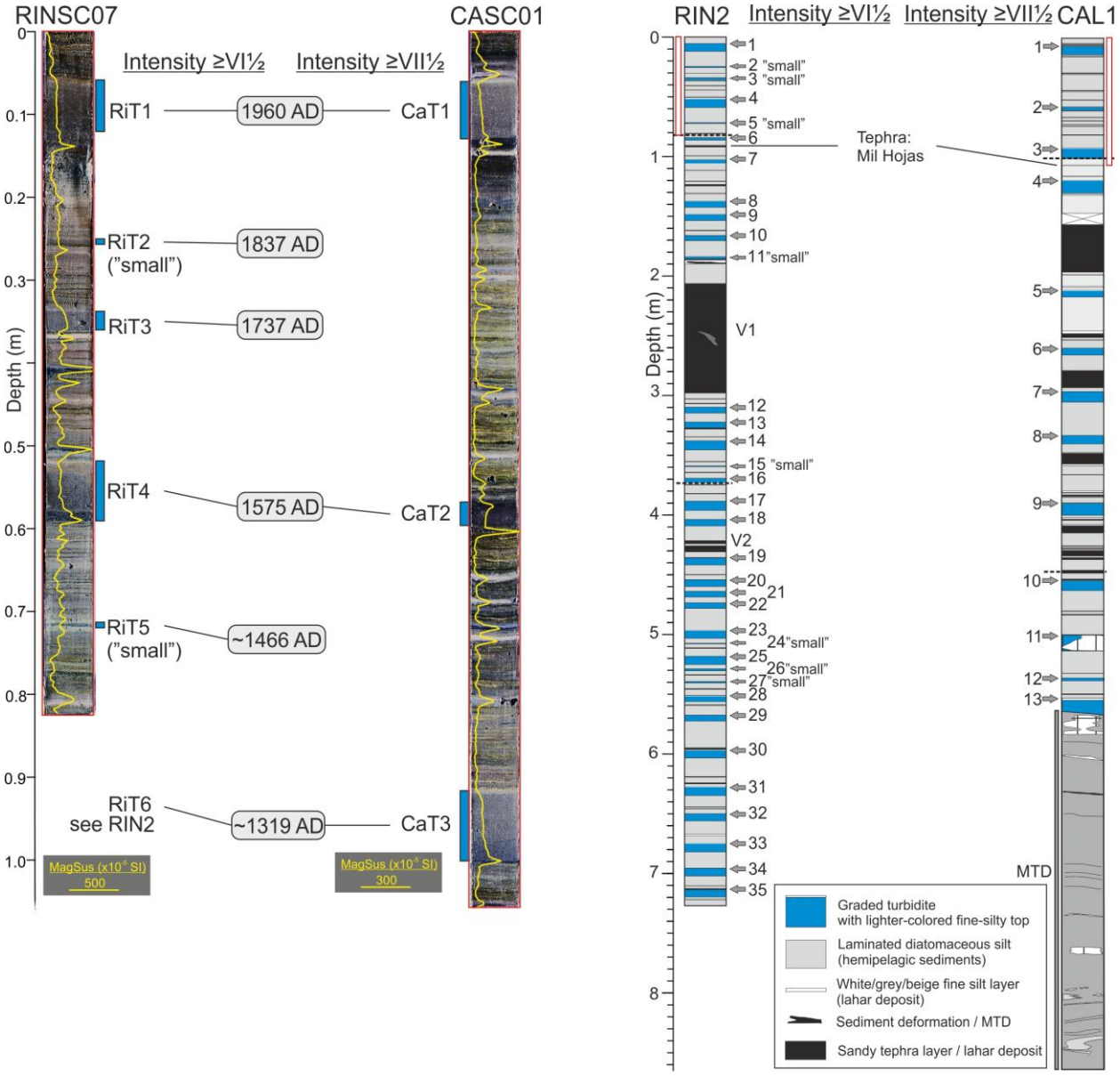

671

672 **Figure 3**

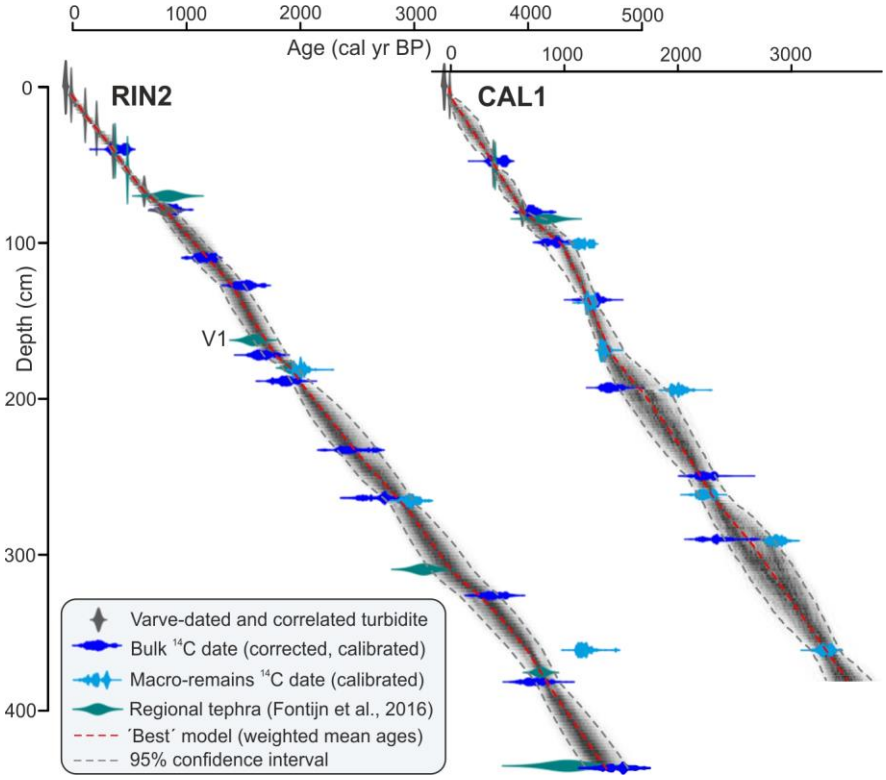

673

674 **Figure 4**

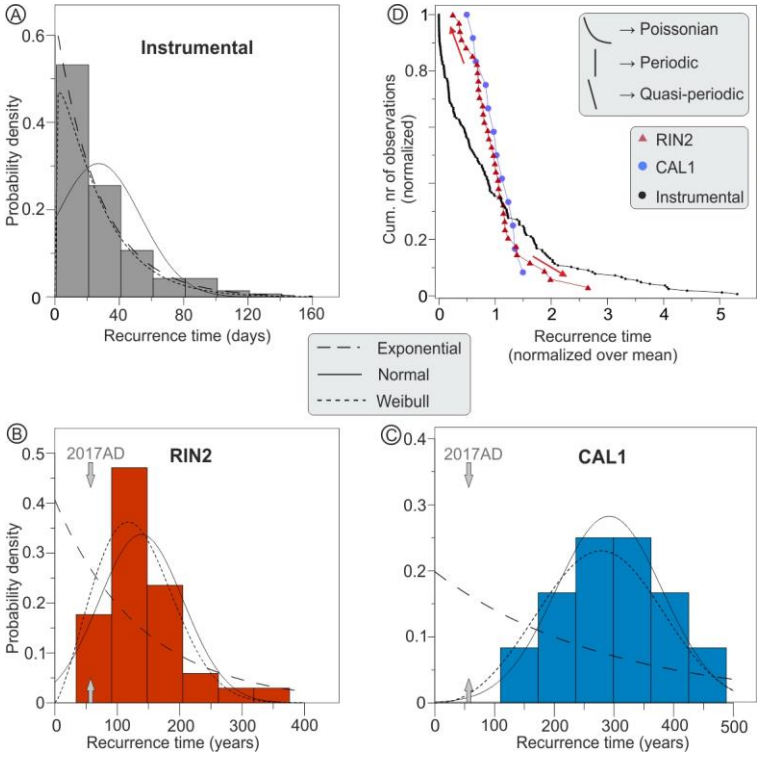

675

676 **Figure 5**

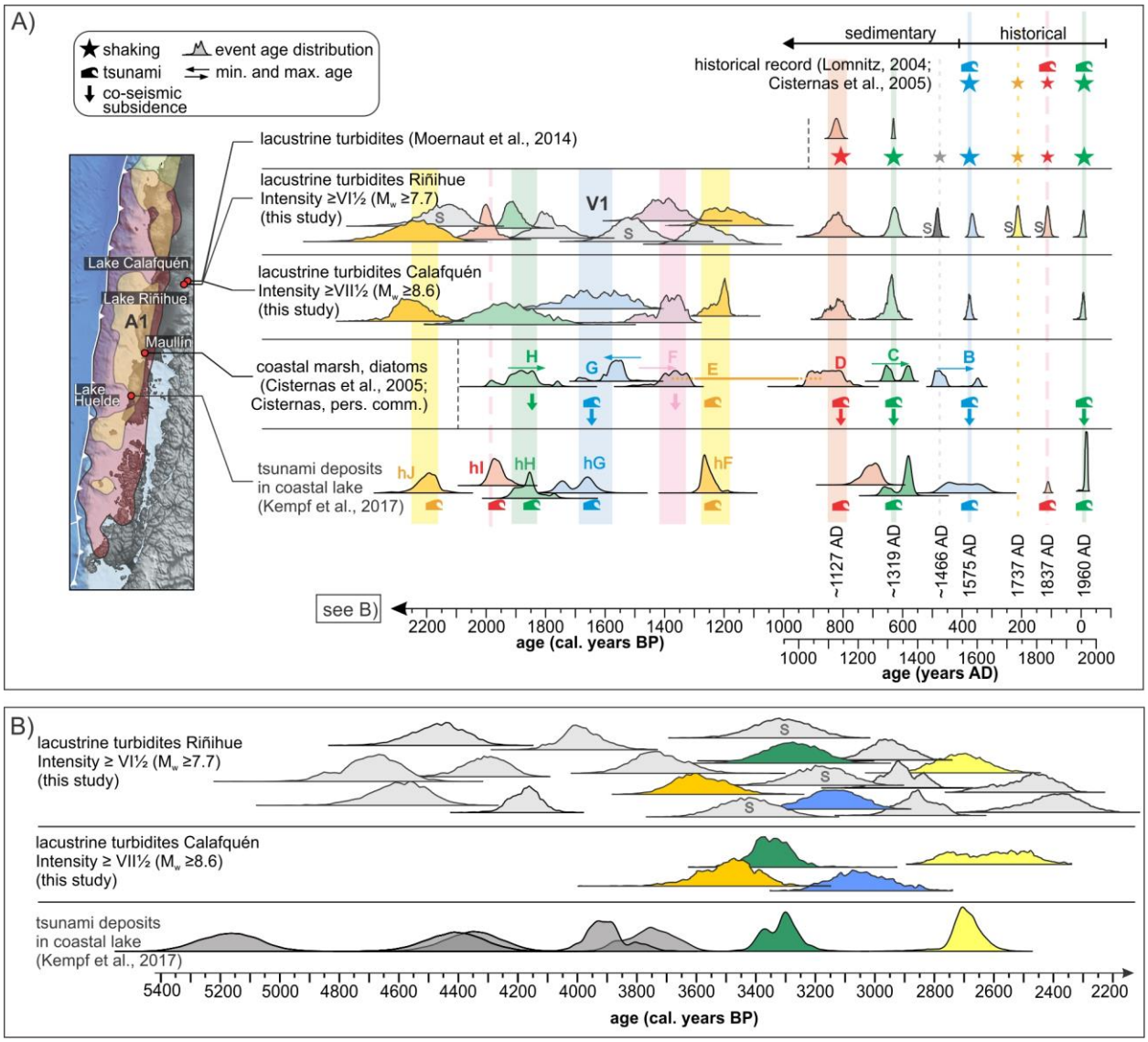

677

678 **Figure 6**

679

680

681 **Table 1**

682

	Instrumental	RIN2	CAL1
Characteristics			
location	36.5-43°S; 70.5-76 °W	Lake Riñihue	Lake Calafquén
unit	days	years	years
minimum (threshold)	$M_w > 4.6$	Intensity ≥ VI½	Intensity ≥ VII½
maximum recorded	M_w 6.6	?	?
observation period	08/1999 – 02/2010	last 4700 yrs	last 3500 yrs
nr. intervals	167	34	12
Descriptive statistics			
median	15.21	125.5	292.2
mean	23.16	138.3	291.8
st dev	25.92	68.5	92.9
COV	1.12	0.50	0.32
Goodness of fit (KS test): Test statistic / p-value			
Exponential	**0.041 / 0.963**	0.317 / 0.003 (R)	0.391 / 0.037 (R)
Normal	0.161 / 0.0012 (R)	0.154 / 0.255	**0.109 / 0.996**
Log-Normal	0.087 / 0.227	0.116 / 0.702	0.119 / 0.988
Weibull	0.059 / 0.699	**0.105 / 0.808**	0.122 / 0.985
Log-Logistic	0.095 / 0.147	0.136 / 0.608	0.159 / 0.877
Interpretation	Poissonian	Quasi-periodic	Quasi-periodic

683

684